THE JOURNAL OF PHYSICAL CHEMISTRY B

ARTICLE

pubs.acs.org/JPCB

Study on Hydroxylammonium-Based Ionic Liquids. I. Characterization

Santiago Aparicio,*[,†] Mert Atilhan,[‡] Majeda Khraisheh,[‡] and Rafael Alcalde[†]

[†]Department of Chemistry, University of Burgos, 09001 Burgos, Spain

[‡]Department of Chemical Engineering, Qatar University, Doha, Qatar

Supporting Information

ABSTRACT: Two selected ammonium-based ionic liquids, 2-hydroxyethyltrimethylammonium L-(+)-lactate and tris(2-hydroxyethyl)methylammonium methylsulfate, were fully characterized. The most relevant thermophysical properties of pure fluids were measured and analyzed as a function of temperature. Structural features were inferred from solvatochromic and Fourier transform infrared (FTIR) studies. Moisture absorption ability was also studied by gravimetric, spectroscopic, and Karl Fischer methods. Likewise, the water effect on fluids properties was analyzed. Polarity was studied by approaches based on solvatochromic measurements and on the water effect on FTIR spectra. Moreover, as computational work, quantum chemistry and molecular dynamics simulation methods were used to analyze the main molecular-level structural features in these fluids. The work is divided into two parts; in this first paper, the main objective is fully characterizing these ionic liquids in the pure state, and in the second paper CO_2 absorption will be analyzed, therefore leading to a deep knowledge of factors controlling structuring, properties, and CO_2 absorption for this family of ionic liquids in comparison with available information for other relevant types of ionic liquids.

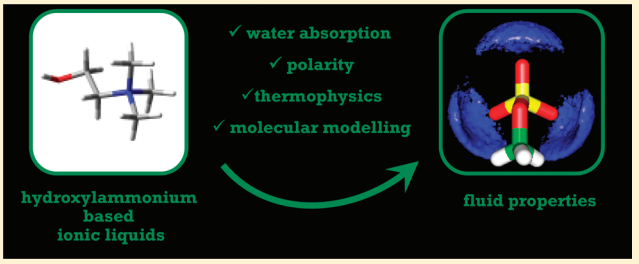

1. INTRODUCTION

The possible use of ionic liquids for CO_2 capture from power plant flue gases has received remarkable attention in recent years, in both industry and academia, as a suitable alternative for traditional absorbents. Several recent works have reviewed the main aspects of the use of ionic liquids for CO_2 capture.[1−4] The available results show promising properties of these fluids. Nevertheless, a long path ahead is required to find suitable candidates that are competitive, both from economical and technological viewpoints, with currently available processes such as the widely used amine-based technologies.[5,6] Likewise, the use of ionic liquids for natural gas sweetening (CO_2 and H_2S capture) has also been proposed in the literature.[4,7] The problems of CO_2 absorption from flue gases and from natural gas for sweetening purposes are different because of the low partial pressure of CO_2 in flue gases, which will require very efficient absorbents, in comparison with large pressures of natural gases.[4] Hence, as stated by Brennecke and Gurkan,[3] ionic liquids leading to physical absorption could be used efficiently for gas sweetening purposes, whereas stronger absorbents (probably only chemical ones) would be required for CO_2 absorption from flue gases. Nevertheless, the molecular-level features controlling CO_2 absorption by ionic liquids, independently of being absorbed from low or high partial pressure gases, are still not fully understood, and available studies are limited to a small number of fluids.

One of the main characteristics of ionic liquids is their flexibility in structure;[3] that is to say, through judicious combinations of anions and cations, we could obtain ionic liquids with tailored properties adequate for the required industrial application.[8−12] This flexibility is an enormous advantage from a technological viewpoint, but it is also a problem from the viewpoint of finding suitable ionic liquids when the large number of possible anion/cation combinations is considered.[13] This phenomenom could be avoided if accurate predictive structure−property relationships were available, for which deep studies on selected families of ionic liquids should be performed to advance understanding of ionic liquids at the molecular level.[14] In the case of CO_2 absorption, these studies should be carried out for ionic liquids with and without absorbed CO_2, to understand molecular-level features controlling absorption and the effect of absorbed CO_2 on ionic liquid structure. Moreover, thermophysical properties are crucial to analyze the suitability of ionic liquids as alternative absorbents; these include viscosity or self-diffusion coefficients, which would control CO_2 absorption kinetics and other relevant features such as pumping or heat and mass transfer processes.[15−17]

The available literature contains analyses of several families of ionic liquids for CO_2 capturing purposes, including cations such as imidazolium,[18,19] phosphonium,[20,21] pyridinium,[22] or guanidinium,[7] paired with anions such as fluorinated ones,[23] acetate,[24] or even anion-functionalized ionic liquids to improve CO_2

Received: July 1, 2011
Revised: August 30, 2011
Published: September 20, 2011

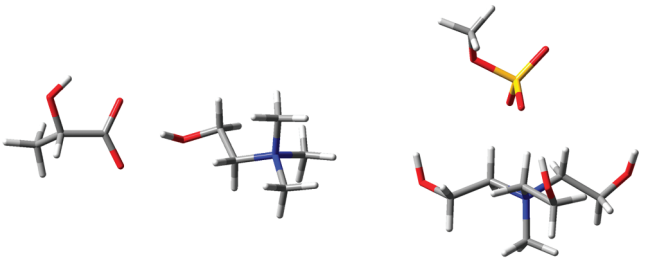

Figure 1. Molecular structures of the studied ionic liquids (ionic pairs), calculated in gas phase at B3LYP/6-311++g** theoretical level.

solubility.[25] Some studies have been reported in the literature about CO_2 absorption in hydroxylammonium-based ionic liquids,[26−28] but to our knowledge, no systematic studies on their structure, properties, and their relationship with CO_2 absorption ability have been reported in the open literature, and thus, we have carried out the study of this family of ionic liquids. This work focuses more on the analyzing the properties of these fluids; a second paper will focus on CO_2 capture performance and properties changes upon CO_2 absorption. Moreover, this work is a continuation of previous studies in which several selected families of ionic liquids were studied by a wide variety of experimental and computational approaches.[7,29−31] Therefore, we have selected two relevant hydroxylammonium-based ionic liquids, 2-hydroxyethyltrimethylammonium L-(+)-lactate ([HE3MA]LAC) and tris(2-hydroxyethyl)methylammonium methylsulfate ([3HEMA]-MS) (Figure 1) and performed an extensive experimental and computational chemistry study for pure and CO_2-absorbed fluids.

The characteristics of ammonium-based ionic liquids are very favorable from environmental and toxicological viewpoints. Nockemann et al.[32] showed the low ecotoxicity of ionic liquids based on the 2-hydroxyethyltrimethylammonium cation (also called choline), and Couling et al.[33] reported that they are significantly less toxic than pyridinium- and imidazolium-based fluids (considering the same anion). For lactate and alkylsulfate anions, we should consider that these or closely related ions have been included in the nontoxic pharmaceutically acceptable and generally recognized as safe (GRAS) ions category for years,[34] and thus they show very good environmental and toxicological profiles. Moreover, from a purely economical viewpoint these fluids may be easily synthesized, leading to lower priced fluids that are competitive with current organic solvents.[26]

Determining and understanding the properties of ionic liquids can be done by using a combined experimental and computational approach as shown in previous works[29−31] and moreover for analysis of the process of CO_2 absorption.[7] This combined approach gives insight into molecular interactions, improves our understanding most effectively, and allows advancement in the development of structure−property relationships, which are crucial for advances in the design and industrial use of ionic liquids. Thermophysical properties such as density, viscosity, speed of sound, refractive index, and conductivity were selected due to their importance for process design purposes and for their close relationship with molecular-level structuring.[35,36] Polarity is a controversial property for ionic liquids;[37−40] several methods have been proposed in the literature to measure it, and thus we have determined polarity based on solvatochromic Reichardt's scale[41] and through the method proposed by Köddermann et al.[39] based on the measurement of FTIR spectra of water dissolved in the studied ionic liquids. Molecular dynamics simulations were performed to obtain a detailed structuring, of the material from energetic and geometric viewpoints.[42] Moreover, several authors have reported both a strong influence of water, both on ionic liquids properties[43,44] and on CO_2 absorption;[45] therefore, this effect was also analyzed in this study. The work is divided into two parts: part I, in which properties of pure fluids were deeply analyzed, and part II, in which CO_2 absorption processes were studied from a computational viewpoint.

2. MATERIALS AND METHODS

2.1. Materials. [HE3MA]LAC (CAS no. 888724-51-4) and [3HEMA]MS (CAS no. 29463-06-7) were obtained from Aldrich; they are colorless viscous fluids. Samples were heated under vacuum for 72 h at 393 K before use and kept under nitrogen atmosphere. Water content was measured through Karl Fischer coulometric titration (Metrohm 831 KF coulometer), with 0.1 g ionic liquid samples, thus leading to ±0.3% accuracy in water mass content.

2.2. Ambient Pressure Thermophysical Properties. Density (ρ) and speed of sound (u) were measured simultaneously with an Anton Paar DSA 5000 instrument, where density was measured by an oscillating U-tube ($\pm 5 \times 10^{-6}$ g·cm^{-3}) and speed of sound by measuring the traveling time of a sound pulse from the piezoelectric transducer to the detector (± 0.5 m·s^{-1}). The cell temperature was controlled by a built-in solid-state thermostat and measured by internal platinum resistance thermometers ($\pm 1 \times 10^{-2}$ K). Calibration was carried out with two reference standards, *n*-nonane (Fluka, purity >99.5%) and toluene (Sigma−Aldrich, purity >99.5%). Density standards for these materials were obtained from the literature.[46]

Dynamic viscosity (η) was measured on an electromagnetic viscometer, VINCI Tech EV1000. The system is built around a measurement chamber in which the sample is placed. A piston inside this chamber is driven electromagnetically through the fluid; two coils move the piston back and forth at a constant force and this traveling time is analyzed and converted into absolute viscosity data. Different piston sizes may be selected depending on the expected sample viscosity. Sample temperature is controlled through an external Julabo F32 circulating bath, and a built-in platinum resistance probe measures the temperature to $\pm 1 \times 10^{-2}$ K. Apparatus calibration was done with certified oils provided by the manufacturer. The accuracy of electromagnetic piston viscometers has been discussed in the literature: Ahosseini and Scurto[47] estimated uncertainty less than 3% when the temperature is controlled by air ovens (±0.1 K), Lundstrum et al.[48] showed 2% uncertainty when proper pistons are used for each viscosity range, and Ragagopal et al.[49] showed 2.4% reproducibility. Considering the uncertainties of pressure and temperature and the fact that suitable pistons were used for each viscosity range, together with analysis of the deviations obtained with certified oils,[50] we concluded and estimated viscosity accuracy of ±2% in the full scale.

Refractive indices (n_D) were measured in relation to the sodium D line by an automated Leica AR600 refractometer to $\pm 5 \times 10^{-6}$. Temperature was controlled by a Julabo F32 external circulator and measured by a platinum resistance thermometer ($\pm 1 \times 10^{-2}$ K). Calibration was performed with double-degassed water (Millipore Milli-Q) and a standard oil (n_D = 1.51416) supplied by the manufacturer.

Conductivity measurements (±1%) were carried out by use of a VWR CO3000L conductivity meter, previously calibrated with KCl standard solutions. Electrode and samples were placed in a sealed glass cell, immersed in a Lauda RE206 bath. The sample temperature (±0.2 K) was measured with a NTC thermistor.

2.3. Spectroscopic Measurements. UV−vis measurements were performed in a Shimadzu UV-1603 spectrophotometer (±0.2 nm) with the temperature of the cell controlled with a Peltier element to $\pm 1 \times 10^{-1}$ K. Reichardt's dye (Aldrich, 95%) was used for solvatochromic measurements according to a procedure previously reported.[51] Attenuated total reflection Fourier transform infrared (ATR-FTIR) spectroscopy studies were developed with a Nicolet Nexus spectrometer together with a Smart Thermal ARK device. The ATR accessory contains a zinc selenide crystal, the temperature of which is controlled through a built-in controller and measured through a RTD temperature sensor to ±1 °C.

2.4. Density Functional Theory Calculations. Density functional theory (DFT) calculations were carried out with the Gaussian 03 package,[52] using the Becke gradient corrected exchange functional[53] and Lee−Yang−Parr correlation functional[54] with three parameters (B3LYP)[55] method. 6-311++g** basis set was used along this work. Atomic charges were calculated to fit the electrostatic potential[56] according to the Merz−Singh−Kollman (MK)[57] scheme. Interaction energies for complexes, ΔE, were calculated as the differences among the complex and sum of monomers' energies at the same theoretical level, with basis-set superposition error (BSSE) corrected through the counterpoise procedure.[58]

2.5. Classical Molecular Dynamics Simulations. Classical molecular dynamics (MD) simulations were carried out with the MDynaMix v 5.0 molecular modeling package.[59] The simulations were carried out in the NPT ensemble, and the Nose−Hoover method was used to control the temperature and pressure of the simulation system.[60] The equations of motion were solved by Tuckerman−Berne double time step algorithm,[61] with long and short time steps of 1 and 0.1 fs, respectively. The Ewald summation method[62] was implemented for Coulombic interactions with a cutoff radius of 1.5 nm. The simulated systems consist of cubic boxes, with the compositions reported in Table S1 (Supporting Information), to which periodic boundary conditions were applied in the three directions to simulate an infinite system. Initial boxes were generated by placing randomly ions, CO_2, and water molecules in a face-centered cubic (fcc) lattice at low density ($\sim$0.2−0.3 g·cm^{-3}), and then NPT simulations were performed at the selected pressure and temperature to ensure equilibration (checked through constant potential energy); after equilibration, 10 ns runs (time step 1 fs) in the NPT ensemble at the studied pressure and temperature were performed for the analysis of systems' properties. Molecules were described according to the force field parametrization described in Table S2 (Supporting Information). Force field parameters for LAC^- and MS^- anions were reported in previous works,[30,31] whereas for $[HE3MA]^+$ and $[3HEMA]^+$ cations, parameters were obtained from Morrow and Maginn.[63] Atomic charges according to the Merz−Singh−Kollman (MK)[57] scheme, obtained as reported in the previous section from gas-phase simulations of isolated ions, were used along the work. The SPC-E model was used for water in this work.[64]

3. RESULTS

3.1. Water Content and Moisture Absorption. Water content of ionic liquids is a property remarkably important because of its effect on relevant thermophysical properties such as viscosity. Moreover, water content may affect CO_2 absorption,[45] and therefore it is extremely important to measure accurately both water content for the samples used and the ability of these fluids to absorb moisture. The water mass percentages for the samples used in this work, measured through Karl Fischer coulometric titration, were 0.81% ± 0.03% and 0.19% ± 0.01% for [HE3MA]LAC and [3HEMA]MS, respectively. Water content for [HE3MA]LAC may seem too high; nevertheless, previous literature studies with this fluid have been carried out with samples with large water content, Machida et al.[65] measured high-pressure densities for [HE3MA]LAC with samples with 0.56% in mass. Moreover, [HE3MA]LAC is a highly hygroscopic fluid, as we will show in this work, and thus, to keep water content at very low levels may require too-complex handling procedures that would increase costs if this fluid were used for industrial purposes. Likewise, [HE3MA]LAC is a highly viscous fluid, as we will show in this work, which is a clear technological disadvantage; this problem may be partially solved by the moisture absorbed, which will decrease the viscosity remarkably in comparison with the ultrapure [HE3MA]LAC. Husson et al.[45] have shown for $[C_2MIM]NTf_2$ ionic liquid that the water effect leads to a 40% decrease in viscosity while maintaining the same order of magnitude of CO_2 solubility.

To get a deeper insight into the absorption of water in the studied ionic liquids, we have carried out measurements for [HE3MA]LAC and [3HEMA]MS moisture absorption ability by several methods. First, samples of each ionic liquid were placed in Petri dishes and exposed to atmospheric moisture (ambient temperature 293 K and 50% relative humidity), and the mass increments upon moisture absorption were gravimetrically measured as a function of time (Figure 2a). Second, the water content of samples exposed to atmospheric moisture was measured through Karl Fischer coulometric titration as a function of exposure time (Figure 2b). Results reported in Figure 2 show remarkable moisture absorption by both ionic liquids, although water absorption ability is larger for [HE3MA]LAC than for [3HEMA]MS. [HE3MA]LAC may capture very large quantities of atmospheric water in short exposures, and thus this fluid should be treated with caution, especially for moisture-sensitive applications. Saturation values obtained through Karl Fischer coulometric titration after 24 h of exposure to atmospheric moisture were 24% and 2.8% for [HE3MA]LAC and [3HEMA]MS, respectively.

Water absorption was also analyzed through ATR-FTIR spectroscopy. Samples of both ionic liquids were placed on the zinc selenide crystal and exposed to atmospheric moisture, at 293 K and 50% atmospheric relative humidity, and the spectra were recorded as a function of time to show water uptake and its effect on the ionic liquids spectra. Results for [HE3MA]LAC are reported in Figure 3. Spectral analysis in the OH-stretching region (3000−3800 cm^{-1}) for [HE3MA]LAC with absorbed water is complicated by the presence in this spectral region of signals rising from the antisymmetric (ν_3) and symmetric (ν_1) stretching modes of water, together with the signal rising from the hydroxyl groups in LAC^- anion and $[HE3MA]^+$ cation. Therefore, to simplify the analysis and thus allow elucidation of the association status of water molecules in [HE3MA]LAC, the spectrum of pure [HE3MA]LAC (t = 0, 0.81% initial water content) was subtracted from all spectra. Results reported in Figure 3 show a wide IR band resembling the pure liquid water band in this region. This wide band discounts the existence of

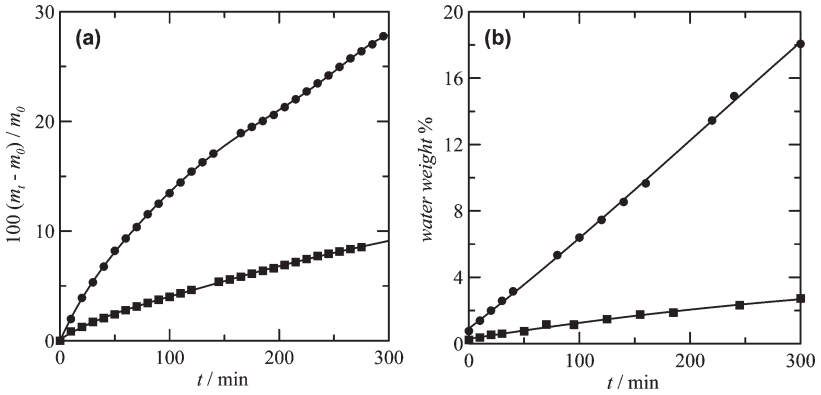

Figure 2. (a) Percentage increment of mass and (b) water weight percentage, measured through Karl Fischer coulometric titration, as a function of time for samples exposed to atmosphere at 293 K and 50% atmospheric relative humidity. Water mass percentages for initial samples were 0.83% and 0.21% for [HE3MA]LAC and [3HEMA]MS, respectively. (●) [HE3MA]LAC; (■) [3HEMA]MS.

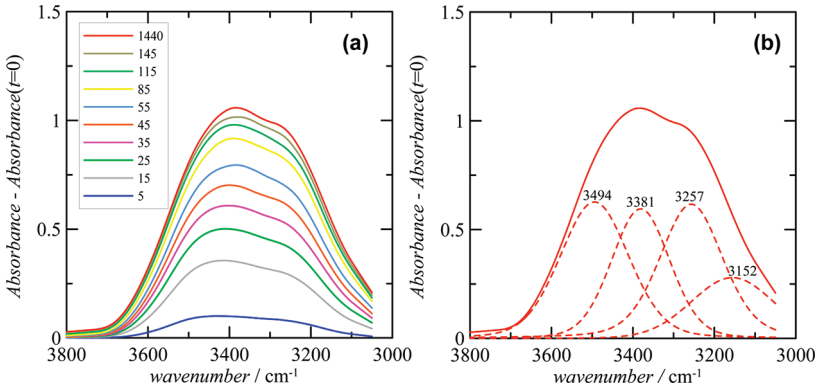

Figure 3. (a) Experimental ATR-FTIR spectra of [HE3MA]LAC, showing water uptake at 293 K and 50% atmospheric relative humidity. Initial sample spectrum of [HE3MA]LAC (t = 0) containing 0.81% water (measured through Karl Fischer coulometric titration) was subtracted from all measurements. Labels within panel a show time in minutes. (b) (—) Total spectrum for t = 1440 min (24 h exposure) and (---) Gaussian−Lorentzian deconvoluted peaks.

free water (not self-associated) and points to the existence of water aggregates probably surrounding hydroxyl groups in both the anion and cation of [HE3MA]LAC ionic liquid. ν_3 and ν_1 modes for water in the vapor state appear at 3756 and 3657 cm^{-1}, and thus the shifting of these bands in [HE3MA]LAC is $\Delta\nu_3$ = 262 cm^{-1} and $\Delta\nu_1$ = 276 cm^{-1} (we assign ν_3 = 3494 cm^{-1} and ν_1 = 3381 cm^{-1}, Figure 3b). These large shifts of ν_3 and ν_1 modes point to strong ion/water interactions, the enthalpies of these hydrogen bonds may be calculated through the expression proposed by Cammarata et al.:[66]

$$\Delta H = -80(\nu_{3,\text{vapor}} - \nu_{3,\text{ionicliquid}})/\nu_{3,\text{vapor}} \quad (1)$$

Therefore, $\Delta H = -24.6$ kJ·mol^{-1} is obtained for the hydrogen-bond strength between ions and water in [HE3MA]LAC. This large affinity between [HE3MA]LAC and water molecules could justify the great moisture absorption ability of this ionic liquid. Moreover, if results reported in this work are compared with those obtained in previous research published by our group for 1-ethyl-3-methylimidazolium lactate ([EMIM]LAC) ionic liquid,[31] analogous results may be inferred, and although the peak structure in the 3000−3800 cm^{-1} spectral region is more complex for [HE3MA]LAC because of the presence of signal rising from the OH groups in $[HE3MA]^+$ cation, water uptake behavior is pretty similar for both fluids. Likewise, analysis of ν_3 mode in [EMIM]LAC led to $\Delta H = -17.5$ kJ·mol^{-1}, and thus, if this result is compared with the value for [HE3MA]LAC, we may infer that most of the water/[HE3MA]LAC interactions are LAC^- anion/water type. Moreover, although water···$[EMIM]^+$ hydrogen bonding in [EMIM]LAC may be developed through the bridging CH group, the additional 7.1 kJ·mol^{-1} in ΔH upon going from [EMIM]LAC to [HE3MA]LAC rises from the stronger $[HE3MA]^+$/water interactions in comparison with $[EMIM]^+$/water interactions. Nevertheless, LAC^- anion/water interactions should develop the main role in water uptake.

The behavior of [3HEMA]MS is very different than that of [HE3MA]LAC. In spite of [3HEMA]MS having three hydroxyethyl chains, which could improve the water−cation interactions in comparison with [HE3MA]LAC, which has a single hydroxyethyl chain, its water affinity is remarkably lower, as shown in Figure 2. This is in agreement with the large LAC−water affinity reported in the previous paragraph, and thus, we may conclude the remarkably lower water affinity of the MS^- anion in comparison with LAC^-. We report the ATR-FTIR results for [3HEMA]MS in Figure 4, in which the signal of pure [3HEMA]MS was subtracted to facilitate analysis. Although reported results show water uptake upon atmospheric exposure, the spectral changes points to weaker ion−water interaction than

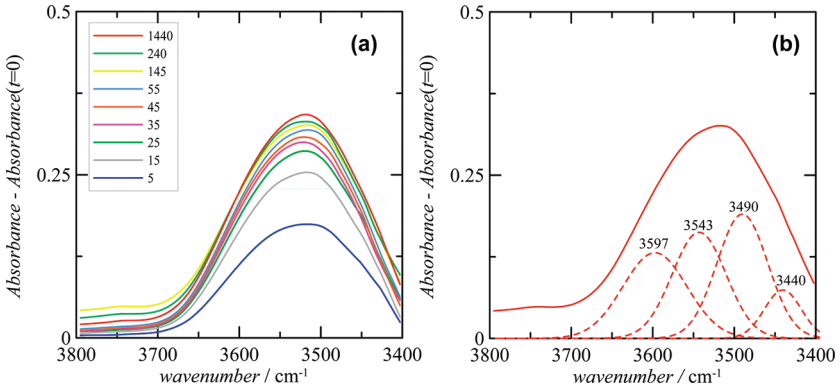

Figure 4. (a) Experimental ATR-FTIR spectra of [3HEMA]MS showing water uptake at 293 K and 50% atmospheric relative humidity. Initial sample spectrum of [3HEMA]MS ($t = 0$) containing 0.19% water (measured through Karl Fischer coulometric titration) was subtracted from all measurements. Labels within panel a show time in minutes. (b) (—) Total spectrum for t = 1440 min (24 h exposure) and (---) Gaussian−Lorentzian deconvoluted peaks.

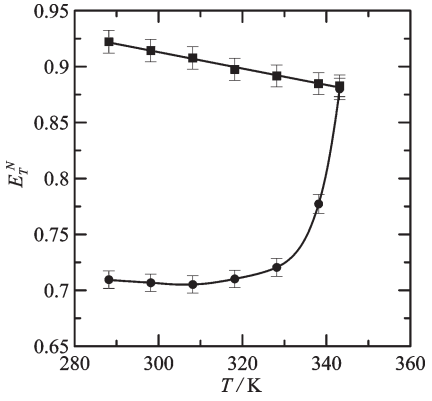

Figure 5. Experimental temperature dependence of E_T^N parameter for (●) [HE3MA]LAC and (■) [3HEMA]MS.

in [HE3MA]LAC. We assign $\nu_3 = 3597\ cm^{-1}$ and $\nu_1 = 3543\ cm^{-1}$ (Figure 4), thus leading to $\Delta\nu_1 = 114\ cm^{-1}$ and $\Delta\nu_3 = 163\ cm^{-1}$, which are remarkably lower shifts than those obtained for water in [HE3MA]LAC, therefore showing the weaker character of hydrogen bonding between water and [3HEMA]MS. Moreover, we obtain $\Delta H = -14.5\ kJ \cdot mol^{-1}$ for [3HEMA]MS by use of eq 1.

3.2. Solvatochromic Parameters, ATR-FTIR Study, and Polarity. In this section, we analyzed the polarity of the studied ionic liquids using two different approaches: (i) Reichardt's polarity scale[41] and (ii) Köddermann's approach[39] in which ATR-FTIR analysis of absorbed water vibrational modes in the OH stretching region led to values of the dielectric constant.

Polarity may be analyzed via the solvatochromic and thermochromic behavior of solutions of the zwitterionic betaine dye 2,6-diphenyl-4-(2,4,6-triphenylpyridinium-1-yl)phenolate (Reichardt's dye) in the studied ionic liquids. The long-wavelength electronic transition of Reichardt's dye depends on the solvent polarity and temperature, showing large hypsochromic shifts with increasing solvent polarity. The $E_T(30)$ and E_T^N solvent polarity parameters may be obtained from the position of the absorption maximum of Reichardt's dye[41] (Table S3, Supporting Information). We report in Figure 5 the thermosolvatochromic behavior of Reichardt's dye in [HE3MA]LAC and [3HEMA]MS ionic liquids, which leads to several relevant conclusions about the polarity of the studied ionic liquids. First, [HE3MA]LAC and [3HEMA]MS ionic liquids are highly polar fluids, especially [3HEMA]MS, for which $E_T^N(298.15\ K) = 0.914$, which is remarkably large in comparison with most of the available ionic liquids of common families such as imidazolium, pyridinium, pyrrolidinium, or phosphonium.[41,67] Second, increasing temperature leads to increasing and decreasing E_T^N parameters for [HE3MA]LAC and [3HEMA]MS, respectively. Decreasing polarity for [3HEMA]MS is the regular behavior we may have expected, but increasing polarity with temperature for [HE3MA]LAC is a highly unusual trend. Nevertheless, Khupse and Kumar[67] recently reported increasing polarity with temperature for phosphonium-based ionic liquids measured also through the E_T^N scale. The unusual behavior of [HE3MA]LAC may be explained by considering the preferential solvation of the excited state of Reichardt's dye, the dipole moment of which is 6 D, by this ionic liquid, in contrast with [3HEMA]MS, which would solvate preferentially the ground state,[67] the polarity of which is 15 D. It could be argued that increasing E_T^N with increasing temperature for [HE3MA]LAC arises from electrolytic properties' growth via dissociation,[67] but simulation results reported in the next sections show that, in the studied temperature range, anion−cation interactions are not remarkably weakened. Therefore, the anomalous behavior of [HE3MA]LAC can be justified only by considering a weakening of the solvent−dye excited-state interactions with increasing temperature for $T > 320$ K (Figure 5), increasing the energy gap between the ground state and excited state of dye molecules and leading to a blue shift in thermosolvatochromism.[67]

We may infer that this different behavior of the two ionic liquids arises mainly from the presence of LAC anion in comparison with MS anion. Nevertheless, E_T^N reported in a previous work for [EMIM]LAC showed lower polarity than [HE3MA]LAC; moreover, [EMIM]LAC showed the usual decreasing E_T^N with increasing temperature, in contrast with [HE3MA]LAC.[31] Therefore, the combination of hydroxylammonium cations and lactate anion leads to very unusual thermosolvatochromic behavior. Likewise, we tried to infer the dielectric constant, ε, for the studied ionic liquids through the relationship between $E_T(30)$ and ε. Köddermann et al.[39] showed that a linear relationship between $E_T(30)$ and ε may be considered; therefore, using this relationship we obtain $\varepsilon = 46$ and 61.3 for [HE3MA]LAC and [3HEMA]MS, respectively. Therefore, according to this approach, these are highly polar liquids, especially

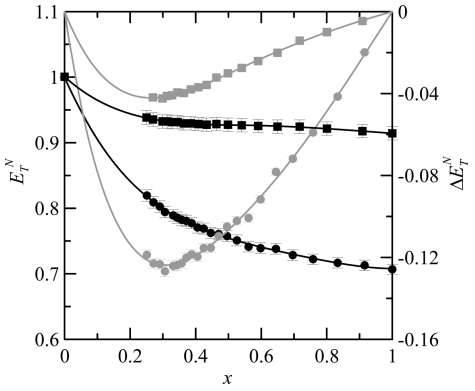

Figure 6. Experimental effect of water on $E_T{}^N$ and $\Delta E_T{}^N$ parameters for x ([HE3MA]LAC or [3HEMA]MS) + $(1 - x)$ water at 298.15 K. (●) [HE3MA]LAC; (■) [3HEMA]MS; (black) $E_T{}^N$; (gray) $\Delta E_T{}^N$; lines are for guiding purposes. Experimental data are reported only for $x >$ 0.25 because of indicator insolubility in water-rich mixtures.

[3HEMA]MS. Nevertheless, Köddermann et al.,[39] and our group in recent work,[31] reported that assuming a linear relationship between $E_T(30)$ and ε is not very reliable, and thus these large ε values have to be confirmed through other approaches. Izgorodina et al.[68] published an analysis on the components of dielectric constants for ionic liquids, showing that ionic liquids with large dipole moments lead to large dielectric constants. Calculated gas-phase dipole moments (at B3LYP/6-311++g** theoretical level) were 3.61, 4.13, 1.70, and 4.08 D for $[HE3MA]^+$, LAC^-, $[3HEMA]^+$, and MS^-, respectively. Therefore, the combination of these anions and cations with large dipole moments would lead to highly polar fluids, which would justify the large ε values obtained from solvatochromic results. Huang et al.[69] have recently published a large collection of experimental dielectric constants for 42 ionic liquids, including hydroxylammonium-based compounds. They showed that hydroxylammonium-based ionic liquids lead to the largest dielectric constants in comparison with common families such as imidazolium, pyridinium, pyrrolidinium, or ammonium. These authors reports $\varepsilon = 85.6 \pm 3.0$ for [HE3MA]LAC, which is remarkably larger than the value obtained from solvatochromic parameters in this work. Nevertheless, the linear correlation between $E_T(30)$ and ε has only a single point for $\varepsilon > 40$, and thus it is not very accurate.[39] Moreover, Huang et al.[69] showed that $\varepsilon = 59.7 \pm 3.0$ for [3HEMA]LAC, and thus increasing the number of hydroxyethyl chains in the cation should lead to lower ε values. Nevertheless, the ε value obtained for [3HEMA]MS from solvatochromic data is larger than that for [HE3MA]LAC, and thus we infer that although solvatochromic measurements are able to predict ε only in a qualitative way, the introduction of MS^- anion should balance the effect of going from $[HE3MA]^+$ to $[3HEMA]^+$.

We have also measured the effect of water addition on the solvatochromic properties of the studied ionic liquid, and thus we report in Figure 6 the $E_T{}^N$ and $\Delta E_T{}^N$ parameters (calculated according to eq 2):

$$\Delta E_T{}^N = E_T{}^N - (x_1 E_{T,1}{}^N + x_2 E_{T,2}{}^N) \quad (2)$$

where x stands for mole fraction and subscripts 1 and 2 represent ionic liquids and water, respectively. Reported results shows increasing $E_T{}^N$ with increasing water mole fraction, but this variation is weak: $E_T{}^N$ increases on going from pure ionic liquids to $x = 0.3$ by 12.3% and 2.6% for [HE3MA]LAC and [3HEMA]MS, respectively. Therefore, the high polarity of these ionic liquids leads to low effects upon water addition, especially for [3HEMA]MS. Only for very large water concentrations ($x_{water} > 0.7$) does $E_T{}^N$ increase remarkably. Moreover, $\Delta E_T{}^N$ is negative for both ionic liquids, which is in agreement with the low effect of water addition on solvatochromic parameters and on polarity, at least in a qualitative way, of these fluids.

Köddermann et al.[39] proposed the use of absorbed water vibrational modes in the OH stretching region to infer values of the dielectric constant as a more reliable method than polarity measurements with solvatochromic probes. The positions of ν_3 and ν_1 water bands were reported in the previous section, which led to $\varepsilon = 49.6$ (from ν_3) and 56 (from ν_1) for [HE3MA]LAC and to $\varepsilon = 26.8$ (from ν_3) and 20.0 (from ν_1) for [3HEMA]MS. ε values for [HE3MA]LAC are in agreement with those obtained from solvatochromic measurements and lower than those reported by Huang et al.[69] ε values for [3HEMA]MS are too low, which may be justified when the difficulty of assigning ν_3 and ν_1 water bands for this ionic liquids through deconvolution of the experimental spectra is considered.

3.3. Thermophysical Measurements. Thermophysical properties (density, speed of sound, refractive index, dynamic viscosity, and conductivity) for the studied ionic liquids are reported in Table S4 (Supporting Information), and plotted in Figure 7 as a function of temperature. [3HEMA]MS is remarkably denser than [HE3MA]LAC (~18%), despite $[3HEMA]^+$ having a larger cation in comparison with $[HE3MA]^+$. Geometrical properties of involved ions were calculated at B3LYP/6-311++g** theoretical level and are reported in Table 1. Sizes and shapes of LAC^- and MS^- anions are almost the same, whereas ovality and size of $[3HEMA]^+$ cation are larger than for $[HE3MA]^+$. Therefore, the larger density of [3HEMA]MS could be explained by considering that geometrical properties of $[3HEMA]^+$ cation allow more efficient packing of MS^- anion in the liquid phase (larger cations lead to larger void spaces in which anions could fit), whereas [HE3MA]LAC leads to less efficient packing because of the smaller size of $[HE3MA]^+$ cation, smaller cations leading to smaller void spaces, which should be rearranged to fit anions. Another remarkable question is the change of density with temperature, or isobaric thermal expansivity (α_p). It is well-known[70] that α_p is very sensitive to the mathematical function used to describe the evolution of density with temperature. We report in Figure 7a the results of fitting experimental density to a linear equation: obtained deviations are within ±0.05% range, which is close to the accuracy of the experimental measurements. Although slightly lower deviations could be obtained by using larger polynomials, we concluded that α_p values obtained from these functions are not very reliable, and thus we considered α_p constant in the studied temperature range, leading to α_p values of 0.56 ± 0.02 and 0.43 ± 0.02 kK^{-1} for [HE3MA]LAC and [3HEMA]MS, respectively. The lower α_p value for [3HEMA]MS points to lower free volume in this ionic liquid in comparison with [HE3MA]LAC, which is in agreement with the behavior of refractive index reported in Figure 7c. Nevertheless, the behavior of speed of sound reported in Figure 7b is highly striking. First, it shows nonlinear behavior for both fluids in the low-temperature region ($T < 298$ K), especially for [HE3MA]LAC. Second, speed of sound for [3HEMA]MS is larger than for [HE3MA]LAC, in spite of the greater density of [3HEMA]MS. Therefore, some fluid rearrangement appears for this low-temperature region leading to that

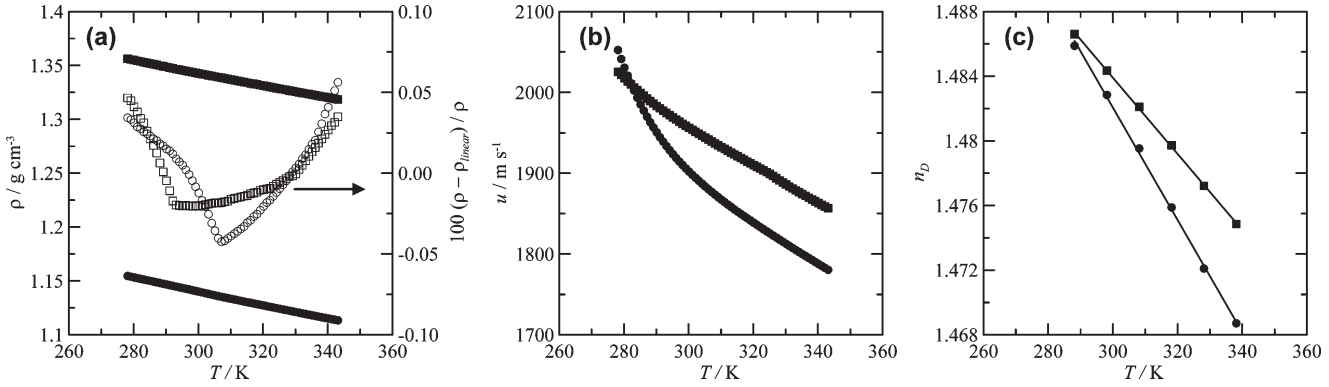

Figure 7. (a) Experimental density ρ, (b) speed of sound u, and (c) refractive index n_D of (●) [HE3MA]LAC and (■) [3HEMA]MS as a function of temperature. In panel a, open symbols show percentage deviations between experimental density and linear fits; in panel c, continuous lines depict linear fits of refractive indices.

Table 1. Properties of Ions Studied in This Work[a]

	ovality	Connolly solvent excluded volume, Å^3
$[HE3MA]^+$	1.16	112.40
LAC^-	1.17	66.56
$[3HEMA]^+$	1.22	155.76
MS^-	1.17	65.23

[a] Calculated in gas phase at B3LYP/6-311++g** theoretical level.

nonlinear behavior. This behavior may be analyzed also by considering the evolution of viscosity and conductivity (Figure 8). Both properties show clear non-Arrhenius behavior, and thus they were fitted to the Vogel−Fulcher−Tamman (VFT) equation:[71]

$$P = P_0 \exp[\pm B/(T - T_0)] \quad (3)$$

where P stands for viscosity or conductivity; P_0, B, and T_0 are fitting parameters; + sign is for viscosity; and − sign is for conductivity. From the VFT parameters reported in Table 2 the fragility parameter, F ($=B/T_0$), defined according to Angell's criteria, may be calculated.[72] [3HEMA]MS and [HE3MA]LAC ionic liquids are highly viscous fluids, which could cause difficulty for some of their possible applications because of the poor heat and mass transfers within these fluids for temperatures close to ambient ones. Nevertheless, viscosity decreases sharply for both fluids, reaching moderate values for temperatures above 333 K (Table S4, Supporting Information). [HE3MA]LAC is more viscous, and thus less conductive, than [3HEMA]MS, except at high temperatures, where there is an inversion (Figure 8a). Results reported in Figure 8b show a clear relationship between viscosity and conductivity for both fluids, leading to almost the same slope in a log−log plot. The larger viscosity of [HE3MA]LAC ionic liquid could be justified by considering the stronger cation−anion interaction in this ionic liquid because of the presence of the hydroxyl group in the anion, which will be analyzed in more detail in the next section. Results reported in Table 2 show that [HE3MA]LAC is more fragile than [3HEMA]MS, according to F values obtained from both viscosity and conductivity. Nevertheless, both fluids show large F values. In a previous work, we reported F = 1.17 and 0.74 (from viscosity and conductivity, respectively) for [EMIM]LAC ionic liquid,[31] and thus we may conclude that hydroxylammonium-based ionic liquids lead to less fragile and, thus, more viscous and less conductive compounds in comparison with common imidazolium-based compounds. This

Table 2. Results of Fits of Experimental Dynamic Viscosity and Conductivity to the VFT Equation[a]

	viscosity		conductivity	
	[HE3MA]LAC	[3HEMA]MS	[HE3MA]LAC	[3HEMA]MS
η_0 or σ_0	0.05[b]	0.04[b]	2830.04[c]	1714.45[c]
B, K	1163.92	1441.80	1140.03	1203.68
T_0, K	189.26	157.77	181.17	159.86
% AAD	1.46	2.83	1.47	1.54
F	6.15	9.14	6.29	7.53

[a] Vogel−Fulcher−Tammann (VFT) equation is eq 3. % AAD stands for the percentage absolute average deviations between experimental and fitted data. F, the fragility parameter, is defined as $F = B/T_0$. [b] η_0, mPa·s. [c] σ_0, S·cm^{-1}.

may be explained by considering the presence of hydroxyl groups in the cation, leading to strong hydrogen bonding between the involved ions.

Walden plots for the relationship between conductivity and viscosity are reported in Figure 9. This method has been applied to analyze the ionization of the studied ionic liquids.[73] In this plot, values for the ionic liquids are compared with the so-called ideal line, corresponding to a solution of ions fully dissociated, and with a line corresponding to 10% ionization. [HE3MA]LAC and [3HEMA]MS fall below the ideal line, approaching that line only at low temperatures. Moreover, the position of both ionic liquids in the Walden plot is almost the same and thus points to a similar degree of ionization. The behavior obtained for both ionic liquids is linear, with a slope of 0.87. In order to quantify the deviations from the ideal reference line, ΔW, defined as vertical deviation from the ideal line, is calculated. ΔW for [HE3MA]LAC evolves from −0.05 at 273.15 K to 0.35 at 368.15 K, whereas ΔW for [3HEMA]MS changes from 0.06 to 0.39 for the same temperature range. The position of both ionic liquids in the Walden plot, approaching the reference line at low temperatures and the 10% ionization line at high temperatures, points to a remarkable effect of temperature on the degree of association.

3.4. Molecular Dynamics Simulations. Analysis of results obtained from MD simulations for the studied ionic liquids would infer relevant conclusions about the microstructural features and dynamic properties of the studied compounds. Validation of results obtained from MD simulations requires a

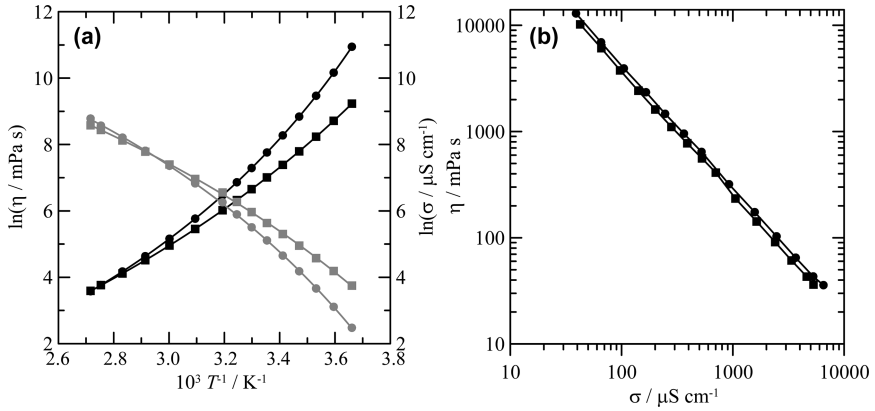

Figure 8. Plots of (a) experimental viscosity η and (b) conductivity σ for (●) [HE3MA]LAC and (■) [3HEMA]MS. In panel a, continuous lines show VFT fits with parameters reported in Table 1, with black symbols and lines for η and gray symbols and lines for σ.

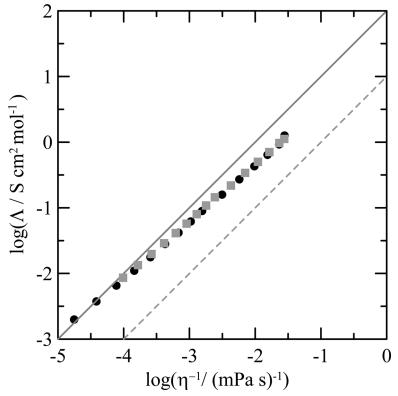

Figure 9. Experimental Walden plot for (●) [HE3MA]LAC and (■) [3HEMA]MS. (—) Ideal line; (---) 10% ionized liquid.

comparison of predicted fluid properties with experimental measurements. We report in Figure S1 (Supporting Information) a comparison between experimental and simulated density data for the studied ionic liquids as a function of temperature. The reported results show deviations in the ±1% range for both fluids, with average absolute deviations of 1% and 0.46% for [HE3MA]LAC and [3HEMA]MS, respectively. Therefore, density predictions may be considered as satisfactory with the proposed force field parametrization. Nevertheless, Maginn[42] considered that density is a mean-field property, and thus it is not very sensitive to changes in force field parametrization; therefore additional properties should also be analyzed. Vaporization enthalpy is a suitable property for validation purposes[42] and it was predicted in this work as well. Gas phase was simulated by considering an isolated neutral pair, because it is well-known that this assumption describes vapor phases of ionic liquids properly.[74] Vaporization enthalpy, ΔH^{vap}, and its closely related property cohesive energy density, c, were obtained from simulations of liquid fluids and gas phase ionic pairs by use of[75]

$$\Delta H^{vap} = (U^{ionpair} - U^{liq}) + RT \quad (4)$$

$$c = \frac{(U^{ionpair} - U^{liq})}{V} \quad (5)$$

where U stands for the average internal energy of ion pair (assuming that it mimics the ideal gas phase) and liquid phase, and V is the liquid molar volume. The different contributions to ΔH^{vap} are reported in Table 3, together with the calculated ΔH^{vap} data. The studied hydroxylammonium ionic liquids show large ΔH^{vap} values, larger for [HE3MA]LAC than for [3HEMA]MS, which is in agreement with the larger anion−cation interaction energies for [HE3MA]LAC reported in Table 3 (21% larger for the electrostatic interaction and only 2.9% for the Lennard-Jones contribution). This behavior may be justified by considering the size of $[3HEMA]^+$, which in spite of having three hydroxyl groups hinders the development of anion and cation interactions. To our knowledge, ΔH^{vap} data have not been measured, and thus comparison with the predicted values reported in this work was not possible. We reported in a previous work ΔH^{vap} = 120.71 kJ·mol^{-1} for hexamethylguanidinium lactate ionic liquid (in fair agreement with experimental data),[7] and thus upon going from the hexamethylguanidinium to $[HE3MA]^+$ cation ΔH^{vap} increases remarkably. This is probably due to the presence of the hydroxyl group in the cation, which may act as a hydrogen-bond donor or acceptor. The split of energy contributions for the studied ionic liquids, in both the liquid and gas phases, shows that Coulombic energy contributions (ELE) are remarkably larger than Lennard-Jones (LJ) ones (only ∼9% LJ contribution to the total liquid phase intermolecular energy), but nevertheless LJ contributions to ΔH^{vap} are very important (33% for [HE3MA]LAC and 45% for [3HEMA]MS). The temperature effect on the different intermolecular interaction energies for both ionic liquids shows an almost linear decrease of all energy contributions with increasing temperature for both ionic liquids for all the ion−ion interactions, as reported in Figure 10. Nevertheless, the weakening of intermolecular interaction energy is only 4.6% and 4.3% for the total Lennard-Jones contribution and 1.3% and 2.5% for the Coulombic contribution for [HE3MA]-LAC and [3HEMA]MS, respectively, in the 273−363 K range. These results point to strong intermolecular interactions, which are not remarkably weakened in the studied temperature range. Moreover, Coulombic intermolecular energies for [3HEMA]MS are lower than for [HE3MA]LAC, whereas the reverse is obtained for Lennard-Jones contributions. Nevertheless, the total intermolecular energies are very similar for both fluids.

Microstructural features were first analyzed by considering radial distribution functions (RDFs). We report in Figure 11 RDFs for the ion centers of mass of both ionic liquids. The main difference between RDFs for [HE3MA]LAC and [3HEMA]MS arises from the hydrogen-bond donor−acceptor ability of LAC^-

Table 3. Lennard-Jones and Electrostatic Energy Contributions to Gas and Liquid Phases of [HE3MA]LAC and [3HEMA]MS and Vaporization Enthalpy at 303 K/2.5 MPa[a]

	intermolecular										
	LJ				ELE						
	A−C	A−A	C−C	total	A−C	A−A	C−C	total	intra	ΔH_{vap}, kJ·mol^{-1}
						[HE3MA]LAC				
liquid	−23.17 ± 0.02	−9.57 ± 0.01	−19.79 ± 0.01	−52.53 ± 0.04	−3179.80 ± 1.01	1307.96 ± 0.86	1299.01 ± 0.45	−572.83 ± 2.32	423.05 ± 0.50	
gas	11.14 ± 0.11			11.14 ± 0.11	−448.07 ± 0.42			−448.07 ± 0.42	425.87 ± 0.26	
gas − liquid				63.67 ± 0.15				124.76 ± 2.74	2.82 ± 0.76	193.77 ± 3.65
						[3HEMA]MS				
liquid	−22.53 ± 0.04	−6.58 ± 0.01	−25.28 ± 0.03	−54.29 ± 0.08	−2631.61 ± 1.47	1031.09 ± 0.87	1028.44 ± 0.80	−572.08 ± 3.14	611.34 ± 0.20	
gas	14.29 ± 0.14			14.29 ± 0.14	−492.36 ± 1.51			−492.36 ± 0.92	614.64 ± 1.99	
gas − liquid				68.58 ± 0.22				79.72 ± 4.06	3.30 ± 2.19	151.60 ± 6.47

[a] Intramolecular contributions (intra) include bonded and non-bonded (LJ + ELEC) interactions. All values are given in kilojoules per mole. A stands for anion and C for cation. Kinetic energy difference between gas and liquid phases is 0.2−0.3 kJ·mol^{-1} for both ionic liquids, and thus it was neglected in the calculation of ΔH_{vap}. All values were obtained from MD simulations.

anion in comparison with MS^- anion, which may act only as a hydrogen-bond acceptor. This is clearly inferred from the anion−anion RDFs reported in Figure 11: two well-defined shells are obtained for [HE3MA]LAC, whereas a broad band without a well-defined peak is obtained for [3HEMA]MS. Cation−cation RDF for [HE3MA]LAC shows a narrow peak, whereas for [3HEMA]MS a wider and weaker peak, with maximum at larger distances, is obtained, which points to weaker interactions between $[3HEMA]^+$ cations in comparison with interactions between $[HE3MA]^+$ cations. This may be justified by considering steric hindrance due to the size of $[3HEMA]^+$, which could make intercationic interaction difficult in spite of having three hydroxyl groups, in comparison with $[HE3MA]^+$. Anion−cation interactions lead to narrow peaks for both ionic liquids, which points to remarkable interactions between these ions. For [3HEMA]MS, anion−cation RDF shows a first narrow peak followed by a shoulder, this may be justified by considering the size of the $[HE3MA]^+$ cation. Results reported in Figure 11 point to the development of anion−cation hydrogen bonding; therefore, we report in Figure 12 site−site RDFs for relevant atomic sites. RDFs reported in Figure 12 for [HE3MA]LAC show the development of cation−cation hydrogen bonding (H4−O1) as well as anion−anion (H7−O2, H7−O3/O4), because of the first peak appearing in the 1.6−1.8 Å range, but these peaks are remarkably weaker than those obtained for the cation−anion interaction through the H4−O2 (hydroxyl−hydroxyl interaction) and H4−O3/O4 (hydroxyl−COO interaction). Therefore, $[HE3MA]^+$ and LAC^- develop strong hydrogen bonding mainly through the COO anion site. For [3HEMA]MS, analogous results were obtained with strong hydrogen bonding between hydroxyl hydrogen in the cation and oxygens of the sulfate group (H4−O6). Spatial distribution functions (SDFs) provide a more detailed viewpoint of cation−anion interaction. We report in Figure 13 the distribution of cation hydroxyl hydrogens (H4) around corresponding anions. SDF for [HE3MA]LAC shown in Figure 13a points to H4 atoms placed surrounding the lactate COO oxygens and a weaker cap above the lactate OH group, which point to a remarkable interaction through these positions. For [3HEMA]MS, Figure 13b, the three caps around the MS SOO group shows a preferred interaction through this site, and the obtained SDF discounts the existence of interactions through the oxygen close to the methyl group in MS.

The effect of temperature on the cation and anion interactions from the RDF viewpoint is almost negligible for the studied temperature range for both ionic liquids. For [HE3MA]LAC, the coordination number for the H4−O2 interactions for the first shell (r = 2.25 Å) is 0.10 ± 0.02, whereas for H4−O3/O4 (r = 2.15 Å) it is 0.45 ± 0.02 for temperatures in the 273−363 K range. For [3HEMA]MS, the coordination for H4−O6 interaction in the first shell (r = 2.35 Å) is 0.29 ± 0.02 for the 273−363 K range. Therefore, no remarkable structural changes are produced in the studied temperature range, which is in agreement with the strong cation and anion interactions reported for both fluids.

Analysis of dynamic properties of hydroxylammonium-based ionic liquids was carried out through the self−diffusion coefficient, D, obtained from Einstein's relationship:

$$D = \frac{1}{6}\lim_{t\to\infty}\frac{\mathrm{d}}{\mathrm{d}t}\langle \Delta r(t)^2\rangle \qquad (6)$$

where the quantity in broken brackets is the mean square displacement (msd). The high viscosity of the studied fluids

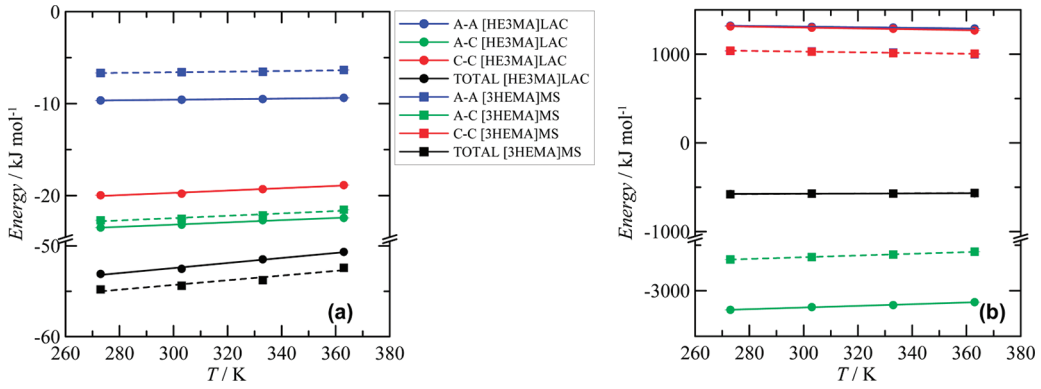

Figure 10. Effect of temperature on (a) Lennard-Jones and (b) Coulombic intermolecular energy contributions for (●) [HE3MA]LAC and (■) [3HEMA]MS ionic liquids obtained from MD simulations. A stands for anion and C for cation. All values were calculated for 2.5 MPa.

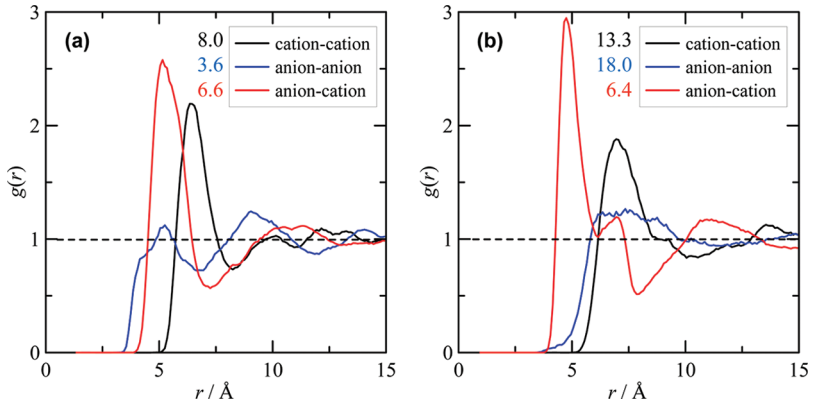

Figure 11. Center-of-mass radial distribution functions, $g(r)$, for (a) [HE3MA]LAC and (b) [3HEMA]MS ionic liquids at 303 K/2.5 MPa, obtained from MD simulations. Numbers within each panel show the coordination numbers of the first solvation shells.

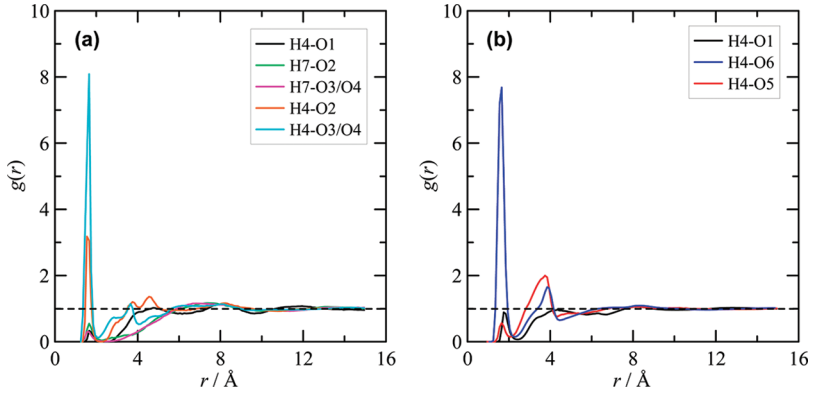

Figure 12. Site−site radial distribution functions, $g(r)$, for (a) [HE3MA]LAC and (b) [3HEMA]MS ionic liquids at 303 K/2.5 MPa, obtained from MD simulations. Atom numbering is as described in Table S2 (Supporting Information).

(Table S3, Supporting Information), especially at low temperatures, requires very long simulations to capture accurately the dynamics of these fluids and to ensure that the fully diffusive regime was reached, and thus that the obtained D values are accurate. The β parameter, defined according to eq 7, is very useful to analyze whether a fully diffusive regime ($\beta = 1$) was reached when msd is studied as a function of simulation time:[7,76]

$$\beta(t) = \frac{\mathrm{d}\log_{10}\langle\Delta r(t)^2\rangle}{\mathrm{d}\log_{10} t} \quad (7)$$

Values of β in the 0.80−0.90 range were obtained for both fluids for simulations at 273−303 K, whereas values in the 0.90−0.95 range were obtained for 333−363 K simulations. Therefore, true D values are probably larger than the ones reported in this work, especially for the simulations at 273 K, for which both fluids are extremely viscous. We report in Figure 14a msd values for cations and anions in both ionic liquids at 303 K/2.5 MPa. Values for [HE3MA]LAC are lower than for [3HEMA]MS, and anions diffuse faster than cations for both ionic liquids. This could be justified by considering the larger sizes of the studied

dx.doi.org/10.1021/jp2062089 |J. Phys. Chem. B 2011, 115, 12473–12486

hydroxylammonium ionic liquids in comparison with the corresponding LAC and MS anions. Temperature effects on calculated D values are reported in Figure 14b. [3HEMA]MS diffuses more rapidly (34.83×10^{-12} and 25.89×10^{-12} $m^2 \cdot s^{-1}$ for anion and cation, respectively, at 303 K/2.5 MPa) than [HE3MA]LAC (4.12×10^{-12} and 2.90×10^{-12} $m^2 \cdot s^{-1}$ for anion and cation, respectively, at 303 K/2.5 MPa), which could be surprising given the larger size of $[3HEMA]^+$ cation. Nevertheless, this could be justified by considering the lower intermolecular interaction energies for [3HEMA]MS reported in Table 3 in comparison with [HE3MA]LAC. Moreover, this behavior would justify the lower viscosities of [3HEMA]MS when compared with [HE3MA]LAC, because of the inverse ratio between viscosity (η) and D coefficients according to the Stokes−Einstein relationship:

$$\eta = \frac{k_B T}{6\pi D r} \tag{8}$$

where k_B stands for the Boltzmann constant, T is temperature, and r is the effective hydrodynamic radius. The main problem for the application of eq 8 to ionic liquids is the value of r. Köddermann et al.[77] have showed that the existence of microheterogeneities, especially for low to moderate temperatures, leads to r values that are temperature-dependent (decreasing with decreasing temperature). Experimental viscosity for [3HEMA]MS (Table S4, Supporting Information) is 236% lower than for [HE3MA]LAC at 283 K, whereas at 353 K it is only 6% lower. Nevertheless, the calculated average self-diffusion coefficients [$D_{IL} = {}^1/_2(D_{anion} + D_{cation})$] are 89−86% larger for [3HEMA]MS than for [HE3MA]LAC in the 273−363 K range, and thus it is not possible to explain viscosity variation with temperature only through the evolution of D_{IL} with temperature.

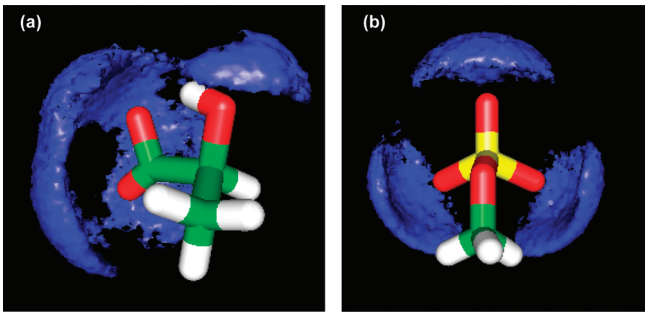

Figure 13. Spatial distribution functions of hydroxyl hydrogens in hydroxylammonium cations (H4 atoms; see Table S2, Supporting Information) around LAC^- and MS^- anions for (a) [HE3MA]LAC and (b) [3HEMA]MS ionic liquids at 303 K/2.5 MPa, obtained from MD simulations. Blue surfaces show 10 times bulk density.

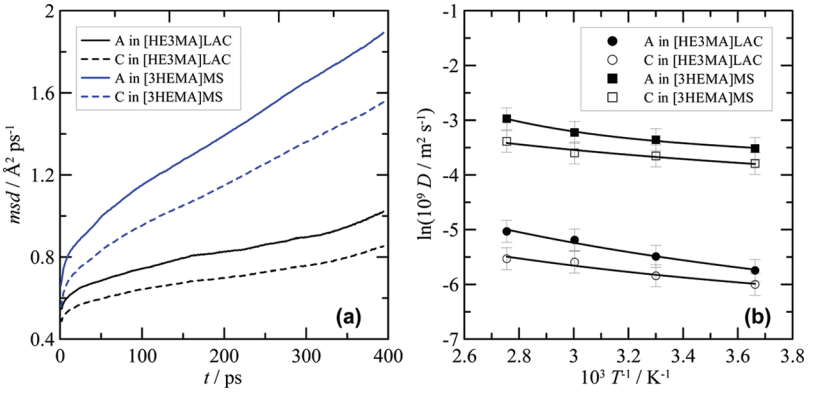

Figure 14. (a) Mean square displacement (msd) at 303 K/2.5 MPa and (b) temperature effect on self-diffusion coefficients (D) for [HE3MA]LAC and [3HEMA]MS. All values in panel b are reported for 2.5 MPa. Continuous lines in panel b shows Vogel−Fulcher−Tamman fits. All values were obtained from MD simulations. A stands for anion and C for cation.

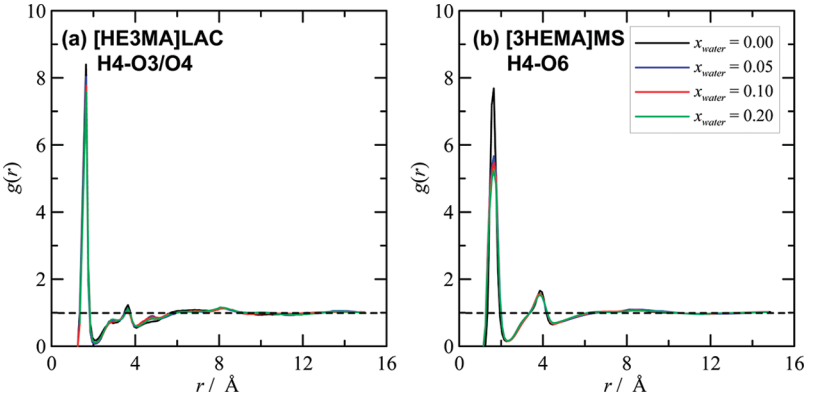

Figure 15. Site−site radial distribution functions, $g(r)$, for x_{water} + (a) [HE3MA]LAC or (b) [3HEMA]MS, at 303 K/2.5 MPa, obtained from MD simulations. Atom numbering is as described in Table S2 (Supporting Information). x_{water} stands for water mole fraction.

dx.doi.org/10.1021/jp2062089 |J. Phys. Chem. B 2011, 115, 12473–12486

We may consider that at low temperatures the viscosity of [HE3MA]LAC is remarkably lower than that of [3HEMA]MS because of the lower intermolecular interaction energies leading to remarkably lower D_{IL} values (diffusion-controlled viscosity). As the temperature increases, the effect of ion sizes begins to be relevant in comparison with intermolecular interactions, and thus the viscosity of the ionic liquid containing the larger cation ([3HEMA]MS) approaches that of [HE3MA]LAC. This could be also justified by the Stokes−Einstein relationship, eq 8, through the nonconstant values of the hydrodynamic radius with temperature that should lead to different viscosity/self-diffusion coefficient ratios for low and high temperatures.

3.5. Computational Study on the Effect of Water on Ionic Liquid Structure. Water has a remarkable effect on the properties of the studied ionic liquids. Therefore, we have performed MD simulations to analyze the effect of water on the microstructural and dynamic properties of these ionic liquids. We have performed simulations for water mole fraction (x_W) equal to 0.05, 0.10, and 0.20 (Table S1, Supporting Information). Site−site RDFs for the interaction between hydroxyl hydrogens in cations (H4; Table S2, Supporting Information) and oxygens in LAC COO site or in MS SOO site are reported in Figure 15. The reported results show a very slight weakening of anion−cation interactions through water addition, especially for [3HEMA]MS. The analysis of ATR experiments reported in section 3.2 led to large values of enthalpies of water···ionic liquid hydrogen bonding, which is in contrast to the low disruption produced with even large water concentration (Figure 15). This apparent contradiction may be justified by considering the SDFs reported in Figure 16, from which we may infer that water interacts with LAC and MS anions in the same region in which hydrogen of cation hydroxyl groups interacts. Nevertheless, the water molecules do not disrupt remarkably the anion−cation interactions, as may be inferred from the comparison of SDFs reported in Figures 13 and 16. Analysis of cation and anion intermolecular interactions shows a moderate weakening with increasing water mole fraction for both ionic liquids (Figure 17), thus confirming that water molecules do not disrupt remarkably the interaction between hydroxylammonium cations and LAC/MS anions. Moreover, cation and anion self-diffusion coefficients reported in Figure 18 show that for [HE3MA]LAC they increase with increasing water mole fraction, as we may expect with the moderate weakening of intermolecular energies reported in Figure 17, whereas for [3HEMA]MS we obtain a decrease and then an increase for both anion and cation. All the reported results show a moderate disrupting effect on the molecular-level structure of the studied ionic liquids, which could justify the water−hydroxylammonium affinity reported in previous sections of this work.

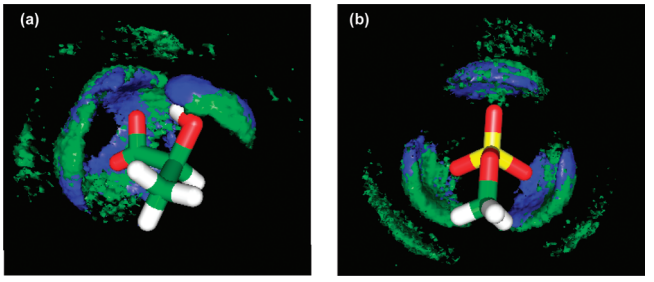

Figure 16. Spatial distribution functions of hydroxyl hydrogens in hydroxylammonium cations (H4 atoms; see Table S2, Supporting Information; blue surfaces) and water hydrogens (HW atoms; see Table S2, Supporting Information; green surfaces) around LAC^- and MS^- anions for x_{water} = 0.20 + (a) [HE3MA]LAC or (b) [3HEMA]MS, at 303 K/2.5 MPa, obtained from MD simulations. Surfaces show 10 times bulk density.

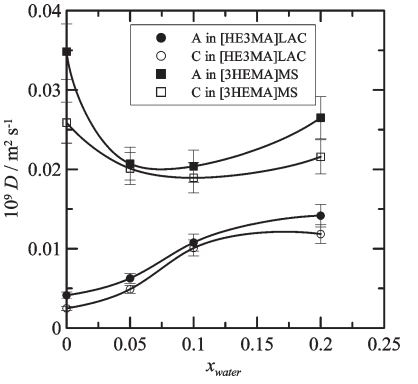

Figure 18. Self-diffusion coefficients (D) for anion and cation in x_{water} + (●, ○) [HE3MA]LAC or (■, □) [3HEMA]MS. All values are reported for 303 K/2.5 MPa. Continuous lines are for guiding purposes. All values were obtained from MD simulations. A stands for anion and C for cation.

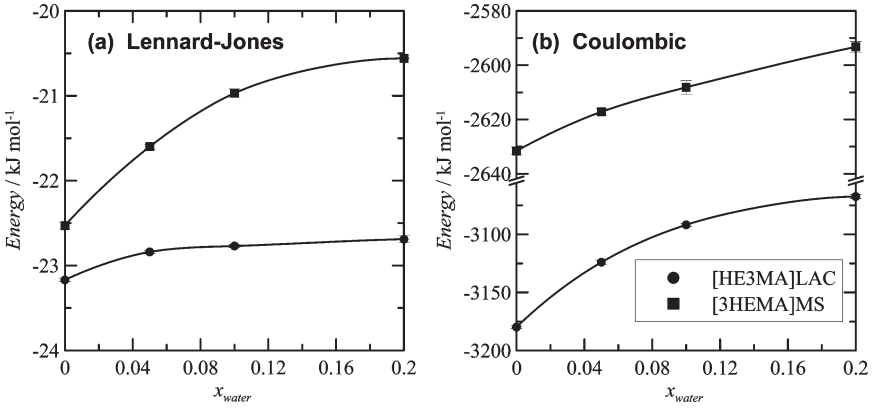

Figure 17. Effect of composition on the anion−cation (a) Lennard-Jones and (b) Coulombic intermolecular energy contributions for x_{water} + (●) [HE3MA]LAC or (■) [3HEMA]MS, obtained from MD simulations. All values were calculated at 303 K/2.5 MPa.

dx.doi.org/10.1021/jp2062089 |J. Phys. Chem. B 2011, 115, 12473–12486

4. CONCLUDING REMARKS

We have reported in this work an extensive experimental and computational study on the properties of hydroxylammonium-based ionic liquids to characterize this fluid for its possible application for CO_2 capture purposes, which will be analyzed in the next part of this series. The reported results lead to several conclusions:

(i) Ionic liquids investigated in this work are highly hygroscopic fluids, especially [HE3MA]LAC, which may be justified by considering the large water−banion affinity through hydrogen bonding.

(ii) [HE3MA]LAC and [3HEMA]MS ionic liquids are highly polar fluids, particularly [3HEMA]MS. The temperature analysis on polarity showed that increasing temperature leads to decreasing polarity for [3HEMA]-MS, which is the regular behavior we may have expected, but to increasing polarity with temperature for [HE3MA]LAC, which is a highly unusual trend.

(iii) Studied fluids are dense fluids, especially [3HEMA]MS. Moreover, these fluids are viscous compounds, particularly [HE3MA]LAC. Substantial viscosity decrease has been observed with increasing temperature for both ionic liquids.

(iv) The reported thermophysical properties points to strong interionic interactions due to the presence of hydrogen-bonding donors and acceptors in the studied ions.

(v) Hydroxylammonium-based ionic liquids are less fragile (and thus more viscous and less conductive) in comparison with common ionic liquids such as imidazolium-based ones. This may be explained by considering the presence of hydrogen bonding between the involved ions.

(vi) The proposed force field parametrization used for MD simulations led to low deviations from experimental properties.

(vii) Large vaporization enthalpies were inferred and a molecular justification of large viscosities and low self-diffusion coefficients through the calculated intermolecular interaction energies was presented.

(viii) Strong cation and anion interactions through specific sites were inferred from the analysis of radial and spatial distribution functions.

(ix) Water absorption does not disrupt remarkably molecular-level structuring.

■ ASSOCIATED CONTENT

Supporting Information. Four tables, showing systems and conditions used for molecular dynamics simulations; force field parameters for $[HE3MA]^+$ and $[3HEMA]^+$ cations, LAC^- and MS^- anions, and water molecules; solvatochromic parameters as a function of temperature; and thermophysical properties of pure ionic liquids as a function of temperature; and one figure, showing comparison between experimental and simulated density data. This material is available free of charge via the Internet at http://pubs.acs.org.

■ AUTHOR INFORMATION

Corresponding Author
*E-mail sapar@ubu.es.

■ ACKNOWLEDGMENT

We acknowledge financial support by Ministerio de Ciencia e Innovación, Spain (Project CTQ2010-15871), and from NPRP Grant NPRP-09-739-2-284 from the Qatar National Research Fund.

■ REFERENCES

(1) Bara, J. E.; Carlisle, T. K.; Gabriel, C. J.; Camper, D.; Finotello, A.; Gin, D. L.; Noble, R. D. *Ind. Eng. Chem. Res.* **2009**, *48*, 2739.
(2) Rahman, M. H.; Siaj, M.; Larachi, F. *Chem. Eng. Process.* **2010**, *49*, 313.
(3) Brennecke, J. F.; Gurkan, B. E. *J. Phys. Chem. Lett.* **2010**, *1*, 3459.
(4) Karadas, F.; Atilhan, M.; Aparicio, S. *Energy Fuels* **2010**, *24*, 5717.
(5) Huang, J.; Rühter, T. *Aust. J. Chem.* **2009**, *62*, 298.
(6) Wappel, D.; Gronald, G.; Kalb, R.; Draxler, J. *Int. J. Greenhouse Gas Control* **2010**, *4*, 486.
(7) Aparicio, S.; Atilhan, M. *Energy Fuels* **2010**, *24*, 4989.
(8) Jork, C.; Kristen, C.; Pieraccini, D.; Stark, A.; Chiappe, C.; Beste, Y. A.; Arlt, W. *J. Chem. Thermodyn.* **2005**, *37*, 537.
(9) Qiu, Z.; Texter, J. *Curr. Opin. Colloid. Interface Sci.* **2008**, *13*, 252.
(10) Armand, M.; Endres, F.; McFarlane, D. R.; Ohno, H.; Scrotasi, B. *Nat. Mater.* **2009**, *8*, 621.
(11) Lu, J.; Yan, F.; Texter, J. *Prog. Polym. Sci.* **2009**, *34*, 431.
(12) Zhou, F.; Liang, Y.; Liu, W. *Chem. Soc. Rev.* **2009**, *38*, 2590.
(13) McLeese, S.; Eslick, J. C.; Hoffmann, N. J.; Scurto, A. M.; Camarda, K. V. Design of Ionic Liquids via Computational Molecular Design. In *Design for Energy and the Environment. Proceedings of the Seventh International Conference on the Foundations of Computer-Aided Process Design*; El-Halwagi, M. M., Linninger, A. A., Eds.; CRC Press: Boca Raton, FL, 2010; p 971.
(14) Weingärtner, H. *Angew. Chem., Int. Ed.* **2008**, *47*, 654.
(15) Ciferno, J. P.; Fout, T. E.; Jones, A. P.; Murphy, J. T. *Chem. Eng. Prog.* **2009**, *105*, 33.
(16) Maginn, E. Evaluation of Ionic Liquids in Post-Combustion CO_2 Capture. 7th Annual Conference on Carbon Capture and Sequestration, Pittsburgh, PA, 2008.
(17) Kilaru, P. K.; Scovazzo, P. *Ind. Eng. Chem. Res.* **2008**, *47*, 910.
(18) Wang, C.; Luo, H.; Luo, X.; Li, H.; Dai, S. *Green Chem.* **2010**, *12*, 2019.
(19) Palgunadi, J.; Kang, J. E.; Cheong, M.; Kim, H.; Lee, H.; Kim, S. *Bull. Korean Chem. Soc.* **2009**, *30*, 1749.
(20) Zhang, Y.; Zhang, S.; Dong, K.; Zhang, Y.; Shen, Y.; Lu, X. *Chem.—Eur. J.* **2009**, *12*, 4021.
(21) Zhang, Y.; Zhang, S.; Lu, X.; Zhou, Q.; Fan, W.; Zhang, X. *Chem.—Eur. J.* **2009**, *15*, 3003.
(22) Supasitmongkol, S.; Styrring, P. *Eng. Environ. Sci.* **2010**, *3*, 1961.
(23) Zhang, X.; Liu, Z.; Wang, W. *AIChE J.* **2008**, *54*, 2717.
(24) Shiflett, M. B.; Drew, D. W.; Cantini, R. A.; Yokozeki, A. *Energy Fuels* **2010**, *24*, 5781.
(25) Gurkan, B. E.; de la Fuente, J. C.; Mindrup, E. M.; Ficke, L. E.; Goodrich, B. F.; Price, E. A.; Schneider, W. F.; Brennecke, J. F. *J. Am. Chem. Soc.* **2010**, *132*, 2116.
(26) Yuan, X. L.; Zhang, S. J.; Lu, X. M. *J. Chem. Eng. Data* **2007**, *52*, 596.
(27) Yuan, X.; Zhang, S.; Liu, J.; Lu, X. *Fluid Phase Equilib.* **2007**, *257*, 195.
(28) Kurnia, K. A.; Harris, F.; Wilfred, C. D.; Mutalib, M. I.; Murugesan, T. *J. Chem. Thermodyn.* **2009**, *41*, 1069.
(29) Dávila, M. J.; Aparicio, S.; Alcalde, R.; García, B.; Leal, J. M. *Green Chem.* **2007**, *9*, 221.
(30) Aparicio, S.; Alcalde, R.; García, B.; Leal, J. M. *J. Phys. Chem. B* **2009**, *113*, 5593.
(31) Aparicio, S.; Alcalde, R.; Atilhan, M. *J. Phys. Chem. B* **2010**, *114*, 5795.
(32) Nockemann, P.; Thijs, B.; Driesen, K.; Jansenn, C. R.; van Hecke, K.; van Meervelt, L.; Kossmann, S.; Kirchner, B.; Binnemans, K. *J. Phys. Chem. B* **2007**, *111*, 5254.
(33) Couling, D. J.; Bernot, R. J.; Docherty, K. M.; Dixon, J. K.; Maginn, E. J. *Green. Chem.* **2006**, *8*, 82.

(34) (a) *Handbook of Pharmaceutical Salts. Properties, Selection and Use*; Stahl, P. H., Wermuth, C. G., Eds.; Wiley−VCH: Weinheim, Germany, 2002. (b) Office of the Federal Register. Direct Food Substances Affirmed As Generally Recognized As Safe. *Code of Federal Regulations. Food and Drugs*, Chapt. 21, Part 184; U.S. Government Printing Office: Washington, DC. http://ecfr.gpoaccess.gov/cgi/t/text/text-idx?c=ecfr&sid=786bafc6f6343634fbf79fcdca7061e1&rgn=div5&view=text&node=21:3.0.1.1.14&idno=21 (accessed March 10, 2011).
(35) Rooney, D.; Jacquemin, J.; Gardas, R. *Top. Curr. Chem.* **2010**, *290*, 185.
(36) Aparicio, S.; Atilhan, M.; Karadas, F. *Ind. Eng. Chem. Res.* **2010**, *49*, 9580.
(37) Wakai, C.; Oleinikova, A.; Ott, M.; Weingärtner, H. *J. Phys. Chem. B* **2005**, *109*, 17028.
(38) Bright, F. V; Baker, G. A. *J. Phys. Chem. B* **2006**, *110*, 5822.
(39) Köddermann, T.; Wertz, C.; Heintz, A.; Ludwig, R. *Angew. Chem., Int. Ed.* **2006**, *45*, 3697.
(40) Singh, T.; Kumar, A. *J. Phys. Chem. B* **2008**, *112*, 12968.
(41) Reichardt, C. *Green Chem.* **2005**, *7*, 339.
(42) Maginn, E. J. *J. Phys.: Condens. Matter* **2009**, *21*, No. 373101.
(43) Cammarata, L.; Kazarian, S. G.; Salter, P. A. *Phys. Chem. Chem. Phys.* **2001**, *3*, 5192.
(44) Kelkar, M. S.; Maginn, E. J. *J. Phys. Chem. B* **2007**, *111*, 4867.
(45) Husson, P.; Pison, L.; Jacquemin, J.; Cost-Gomes, M. F. *Fluid Phase Equilib.* **2010**, *294*, 98.
(46) Lemmon, E. W.; McLinden, M. O.; Friend, D. G. Thermophysical Properties of Fluid Systems. In *NIST Chemistry WebBook*; NIST Standard Reference Database Number 69; Linstrom, P. J., Mallard, W. G., Eds.; National Institute of Standards and Technology: Gaithersburg, MD, June 2005; http://webbook.nist.gov.
(47) Ahosseini, A.; Scurto, A. M. *Int. J. Thermophys.* **2008**, *29*, 1222.
(48) Lundstrum, R.; Goodwin, A. R.; Hsu, K.; Frels, M.; Caudwell, D. R.; Trusler, J. P. M.; Marsh, K. N. *J. Chem. Eng. Data* **2005**, *50*, 1377.
(49) Rajagopal, K.; Andrade, L. P. R.; Paredes, M. L. L. *J. Chem. Eng. Data* **2009**, *54*, 2967.
(50) Bandrés, I.; Alcalde, R.; Lafuente, C.; Atilhan, M.; Aparicio, S. *J. Phys. Chem. B* (submitted for publication).
(51) García, B.; Aparicio, S.; Alcalde, R.; Ruiz, R.; Dávila, M. J.; Leal, J. M. *J. Phys. Chem. B* **2004**, *108*, 3024.
(52) Frisch, M. J.; Trucks, G. W.; Schlegel, H. B.; Scuseria, G. E.; Robb, M. A.; Cheeseman, J. R.; Montgomery, J. A., Jr.; Vreven, T.; Kudin, K. N.; Burant, J. C.; Millam, J. M.; Iyengar, S. S.; Tomasi, J.; Barone, V.; Mennucci, B.; Cossi, M.; Scalmani, G.; Rega, N.; Petersson, G. A.; Nakatsuji, H.; Hada, M.; Ehara, M.; Toyota, K.; Fukuda, R.; Hasegawa, J.; Ishida, M.; Nakajima, T.; Honda, Y.; Kitao, O.; Nakai, H.; Klene, M.; Li, X.; Knox, J. E.; Hratchian, H. P.; Cross, J. B.; Adamo, C.; Jaramillo, J.; Gomperts, R.; Stratmann, R. E.; Yazyev, O.; Austin, A. J.; Cammi, R.; Pomelli, C.; Ochterski, J. W.; Ayala, P. Y.; Morokuma, K.; Voth, G. A.; Salvador, P.; Dannenberg, J. J.; Zakrzewski, V. G.; Dapprich, S.; Daniels, A. D.; Strain, M. C.; Farkas, O.; Malick, D. K.; Rabuck, A. D.; Raghavachari, K.; Foresman, J. B.; Ortiz, J. V.; Cui, Q.; Baboul, A. G.; Clifford, S.; Cioslowski, J.; Stefanov, B. B.; Liu, G.; Liashenko, A.; Piskorz, P.; Komaromi, I.; Martin, R. L.; Fox, D. J.; Keith, T.; Al-Laham, M. A.; Peng, C. Y.; Nanayakkara, A.; Challacombe, M.; Gill, P. M. W.; Johnson, B.; Chen, W.; Wong, M. W.; Gonzalez, C.; Pople, J. A. Gaussian 03 (Revision C.02); Gaussian, Inc., Wallingford CT, 2004.
(53) Becke, A. D. *Phys. Rev. A* **1988**, *38*, 3098.
(54) Lee, C.; Yang, W.; Parr., R. G. *Phys. Rev. B* **1988**, *37*, 785.
(55) Becke, A. D. *J. Chem. Phys.* **1993**, *98*, 5648.
(56) Singh, U. C.; Kollman, P. A. *J. Comput. Chem.* **1984**, *5*, 129.
(57) Besler, B. H.; Merz, K. M.; Kollman, P. A. *J. Comput. Chem.* **1990**, *11*, 431.
(58) Simon, S.; Duran, M.; Dannenberg, J. J. *J. Chem. Phys.* **1996**, *105*, 11024.
(59) Lyubartsev, A. P.; Laaksonen, A. *Comput. Phys. Commun.* **2000**, *128*, 565.
(60) Hoover, W. G. *Phys. Rev. A* **1985**, *31*, 1695.
(61) Tuckerman, M.; Berne, B. J.; Martyna, G. J. *J. Chem. Phys.* **1992**, *97*, 1990.
(62) Essmann, U. L.; Perera, M. L.; Berkowitz, T.; Darden, H.; Lee, H.; Pedersen, L. G. *J. Chem. Phys.* **1995**, *103*, 8577.
(63) Morrow, T. I.; Maginn, E. J. *Fluid Phase Equilib.* **2004**, *217*, 97.
(64) Berendsen, H. J. C.; Grigera, J. R.; Straatsma, T. P. *J. Phys. Chem.* **1987**, *91*, 6269.
(65) Machida, H.; Taguchi, R.; Sato, Y.; Smith, R. *J. Chem. Eng. Data* **2011**, *56*, 923.
(66) Cammarata, L.; Kazarian, S. G.; Salter, P. A.; Welton, T. *Phys. Chem. Chem. Phys.* **2001**, *3*, 5192.
(67) Khupse, N. D.; Kumar, A. *J. Phys. Chem. B* **2010**, *114*, 376.
(68) Izgorodina, E. I.; Forsyth, M.; MacFarlane, D. R. *Phys. Chem. Chem. Phys.* **2009**, *11*, 2452.
(69) Huang, M. M.; Jiang, Y.; Sasisanker, P.; Driver, G. W.; Weingärtner, H. *J. Chem. Eng. Data* **2011**, *56*, 1494.
(70) (a) Cerdeiriña, C. A.; Tovar, C. A.; González-Salgado, D.; Carballo, E.; Romaní, L. *Phys. Chem. Chem. Phys.* **2001**, *3*, 5230. (b) Troncoso, J.; Cerdeiriña, C. A.; Navia, P.; Sanmamed, A.; González-Salgado, D.; Romaní, L. *J. Phys. Chem. Lett.* **2010**, *1*, 211.
(71) (a) Zhang, Z. Z.; Chang, Z.; Xu, K.; Angell, C. A. *Electrochim. Acta* **2000**, *45*, 1229. (b) Anouti, M.; Caillon, M.; Le Floch, C.; Lemordant, D. *J. Phys. Chem. B* **2008**, *112*, 9412.
(72) Angell, C. A. *Science* **1995**, *267*, 1924.
(73) MacFarlane, D. R.; Forsyth, M.; Izgorodina, E. I.; Abbott, A. P.; Annat, G.; Fraser, K. *Phys. Chem. Chem. Phys.* **2009**, *11*, 4962.
(74) (a) Leal, J. P.; Esperança, J. M. S. S.; Minas da Piedade, M. E.; Canongia-Lopes, J. N.; Rebelo, L. P. N.; Seddon, K. R. *J. Phys. Chem. A* **2007**, *111*, 6176. (b) Gross, J. H. *J. Am. Soc. Mass Spectrom.* **2008**, *19*, 1347.
(75) Liu, Z. P.; Huang, S. P.; Wang, W. C. *J. Phys. Chem. B* **2004**, *108*, 12978.
(76) (a) Del-Popolo, M. G.; Voth, G. A. *J. Phys. Chem. B* **2004**, *108*, 1744. (b) Hu, Z.; Margulis, C. *Proc. Natl. Acad. Sci. U.S.A.* **2006**, *103*, 831.
(77) Köddermann, T.; Ludwig, R.; Paschek, D. *ChemPhysChem* **2008**, *9*, 1851.